

Drosophila awd, the homolog of human *nm23*, regulates FGF receptor levels and functions synergistically with *shi/dynammin* during tracheal development

Vincent Dammai, Boris Adryan, Kim R. Lavenburg, and Tien Hsu¹

Department of Pathology and Laboratory Medicine, and Hollings Cancer Center, Medical University of South Carolina, Charleston, South Carolina 29425, USA

Human *nm23* has been implicated in suppression of metastasis in various cancers, but the underlying mechanism of such activity has not been fully understood. Using *Drosophila* tracheal system as a genetic model, we examined the function of the *Drosophila* homolog of *nm23*, the *awd* gene, in cell migration. We show that loss of *Drosophila awd* results in dysregulated tracheal cell motility. This phenotype can be suppressed by reducing the dosage of the chemotactic FGF receptor (FGFR) homolog, *breathless (btl)*, indicating that *btl* and *awd* are functionally antagonists. In addition, mutants of *shi/dynammin* show similar tracheal phenotypes as in *awd* and exacerbate those in *awd* mutant, suggesting defects in vesicle-mediated turnover of FGFR in the *awd* mutant. Consistent with this, Btl-GFP chimera expressed from a cognate *btl* promoter-driven system accumulate at high levels on tracheal cell membrane of *awd* mutants as well as in *awd* RNA duplex-treated cultured cells. Thus, we propose that *awd* regulates tracheal cell motility by modulating the FGFR levels, through a dynammin-mediated pathway.

[Keywords: *awd/nm23*; *btl*/FGFR; *shi/dynammin*; tracheal development; *Drosophila*; cell migration]

Supplemental material is available at <http://www.genesdev.org>.

Received March 25, 2003; revised version accepted September 9, 2003.

Human *nm23* encodes a nucleoside diphosphate kinase (NDPK) with tumor metastasis suppressing activity (Steeg et al. 1988). Reduced levels of *nm23* expression correlate with high metastatic potential of certain tumors, including breast carcinoma and melanoma (Steeg et al. 1988; Freije et al. 1997). Conversely, overexpression of Nm23 can reduce the metastatic potential of these tumor cells in vivo (Kantor et al. 1993; Leone et al. 1993; MacDonald et al. 1996). There are eight related *nm23* gene products in human (Nm23H1–H8) and two of them (Nm23H1 and H2) have been widely studied (for reviews, see Lacombe et al. 2000; Roymans et al. 2002). The two proteins are 88% identical. The *Drosophila awd* (abnormal wing disc) gene product is the homolog of Nm23H1/2 and is the source for about 98% of the NDPK activity in embryos (Biggs et al. 1990). It is 78% identical to either Nm23H1 or Nm23H2. Earlier studies showed that loss-of-function *awd* mutants exhibited early pupal lethality in part due to defects in imaginal disc develop-

ment (hence the name; Biggs et al. 1988; Dearolf et al. 1988). Interestingly, the first known allele of *awd*, *killer of prune (K-pn)*, confers lethality to the otherwise benign eye color mutation *prune* (Biggs et al. 1988). It has been suggested that *K-pn* may acquire ectopic substrate or cofactor specificity that exacerbates the underlying defects in mutated *prune* (Timmons and Shearn 2000), which encodes a GTPase activating protein (GAP)-like protein (Teng et al. 1991; Aravind and Koonin 1998).

The human Nm23 proteins display isotype-specific functions. For example, Nm23H1, but not H2, exhibits a single-stranded DNase activity that is activated by cytotoxic T cell-delivered granzyme A and presumably mediates apoptosis in the target cell (Fan et al. 2003). On the other hand, the lethality of *awd* embryos can be rescued by human *nm23H2* but not *H1* (Xu et al. 1996). Therefore, *nm23* genes may be involved in various cellular functions relevant to different aspects of tumor progression.

One potential role for Nm23 as a metastasis inhibitor is regulation of cell motility (Roymans et al. 2002). We suspect that if Nm23 is involved in cell migration events, many of the developmental consequences arising

¹Corresponding author.

E-MAIL hsut@musc.edu; FAX (843) 792-3940.

Article and publication are at <http://www.genesdev.org/cgi/doi/10.1101/gad.1096903>.

from lack of coordination during cell migration should be apparent in *awd* mutants and *awd* should genetically interact with the specific pathways that are activated in those subsets of migrating cells.

The *Drosophila* tracheal system is an excellent model for studying guided cell migration. The tracheal system arises from clusters of ectodermal cells (10 on each side of embryonic segments). Each cluster invaginates from the ectoderm and forms an epithelial sac termed tracheal placode of ~80–100 cells. After formation of tracheal placodes, the entire tracheal system is constructed by coordinated cell migration without further cell divisions (Manning and Krasnow 1993; Metzger and Krasnow 1999). The major chemotactic signaling that guides tracheal tube migration is mediated by the *Drosophila* FGFR encoded by *breathless* (*btl*; Glazer and Shilo 1991; Lee et al. 1996; Ohshiro and Saigo 1997). Guided cell migration is achieved by expression of Branchless (Bnl; FGF homolog) from the surrounding mesoderm and target organs such as the guts (Sutherland et al. 1996). Forced expression of *bnl* can redirect tracheal cells to the ectopic source (Sutherland et al. 1996; Ribeiro et al. 2002) whereas in the absence of Bnl no tracheal migration or fusion of tracheal tubes is observed (Sutherland et al. 1996; Wolf et al. 2002).

Here we investigate the role of *awd* during tracheal tube formation and report novel findings that *awd* controls tracheal cell migration by modulating the levels of Btl/FGFR. In *awd* mutants, the Btl/FGFR levels are dramatically increased on the cell surface. Consequently, ectopic activation of downstream pathways and abnormal migration are evident in tracheal cells of *awd* mutants. Furthermore, the *awd* phenotypes are exacerbated

by mutation in the *Drosophila* *dynamain* gene, *shibire* (*shi*; van der Bliek and Meyerowitz 1991). Taken together, these results show that *awd* is involved in attenuation of Btl/FGFR activity by vesicle-transport-mediated turnover, thus directly influencing tracheal cell motility. This is the first direct *in vivo* demonstration of *awd/nm23* participation in a major RTK pathway that is crucial for controlled cell migration.

Results

awd is expressed in tracheal cells and is required for proper cell migration

We generated polyclonal antibodies against *Drosophila* Awd using bacterially expressed His-tagged version of Awd. The protein A affinity-purified antibody recognizes a single band slightly larger than the 17-kD marker in Western blots of protein extracts from *Drosophila* embryos and *Drosophila* S2 cell line (Fig. 1A). The apparent size is in agreement with the calculated molecular weight, 19.2 kD, of the Awd protein. This antiserum was then used to detect the *in vivo* expression pattern. *awd* RNA has been detected in multiple tissues (Dearolf et al. 1988). To better identify possible expression of Awd protein in the tracheal system, we utilized a reporter transgenic line *1-eve-1* that expresses *lacZ* in all tracheal cells (Perrimon et al. 1991). The *lacZ* insertion does not cause tracheal defects and the *1-eve-1* line will be used as wild type (Wilk et al. 1996; also see below). Immunostaining of *1-eve-1* embryos with anti- β -Gal and anti-Awd antibodies showed that Awd is expressed at low levels in most of the embryonic cells and at high levels in the

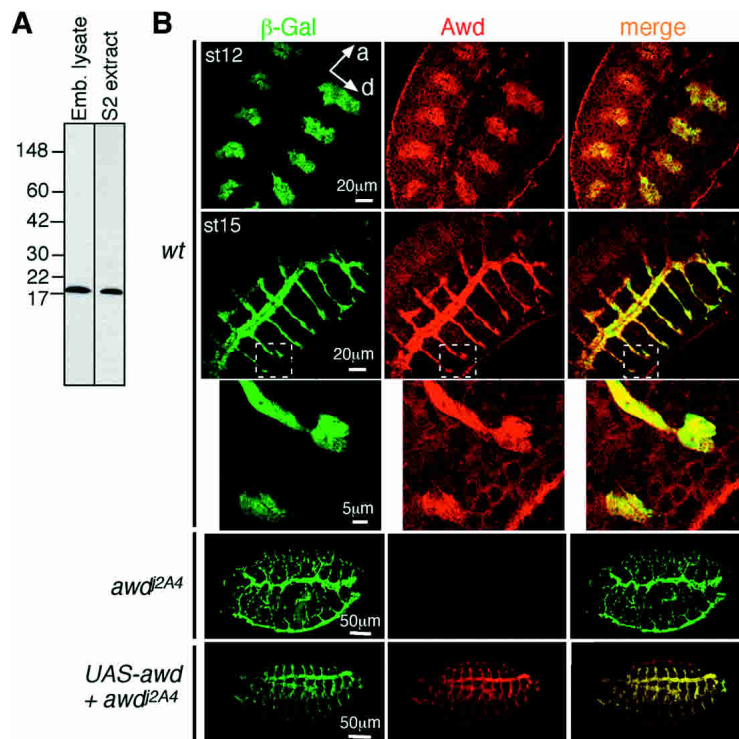


Figure 1. Awd expression in tracheal cells. (A) Affinity-purified rabbit polyclonal antibody against *Drosophila* Awd recognizes a single band by Western blotting in whole embryo and *Drosophila* S2 cell lysates. (B) The same antibody was used to detect Awd expression (red) *in vivo*. The genotypes of the embryos are *1-eve-1* (*wt*); *y, w; 1-eve-1, awd^{2A4}* (*awd*); and *y, w; btl-GAL4, UAS-awd; 1-eve-1, awd^{2A4}* (*UAS-awd + awd*). Tracheal cells were visualized by mouse monoclonal anti- β -Gal staining (green). Arrows in the *top left* panel mark the anterior (*a*) and dorsal (*d*) sides of all the embryos shown. The *top* two rows of images are projections of five 1.5- μ m confocal sections and the close-up images are single sections. The *bottom* two rows are projections of five 2- μ m sections. The two channels were recorded sequentially to avoid bleed-through.

Dammai et al.

tracheal cells (Fig. 1B). It is worth noting that concentrated Awd staining in the trachea was observed only when the embryos were freshly prepared, treated with 0.5% Nonidet-P40, and handled gently. Examples of stage 12 and stage 15 embryos are shown in Figure 1B; however, tracheal expression of Awd is detected as early as placode formation and persists until the entire tracheal system is constructed at stage 17 (data not shown). Note that Awd is a constituent in all tracheal cells examined, suggesting that chemotactic or other temporally and spatially specific signaling events do not regulate its expression.

We next examined the potential tracheal phenotypes in *awd* mutant. Three independently isolated alleles were analyzed. (1) *awd^{j2A4}*, in the *Drosophila* Genome Project collection, has been characterized as a protein-null allele resulting from P-element insertion in the 5' untranslated region (Krishnan et al. 2001). (2) *awd^{KRS6}* is a 788-bp deletion that removes the entire coding region (Timmons et al. 1993, 1995). (3) *Df(3R)awd^{KRB}* is a small chromosome deficiency (100D1: 100D3–4) encompassing *awd* (at 100D2). The embryos were stained with a tracheal lumen-specific monoclonal antibody 2A12. As shown in Figure 2A, stage 16 wild-type embryo shows a stereotypical tubule network. By contrast, all three *awd* alleles show a complex array of abnormalities. These include major disruption of the tracheal network accompanied by ectopic branching and looping (Fig. 2D,G), appearance of a few extra branches or “knobs” (Fig. 2E,F), and migration abnormalities (Fig. 2H,I). All three homozygous *awd* alleles show 75%–80% phenocopies. As shown in Supplementary Table 1, the penetrance can be rescued (down to 11%–15%) by a wild-type *awd* transgene expressed in the tracheal cells using the *btl*-enhancer-directed UAS/GAL4 binary system (Fig. 1B). These tracheal defects in *awd* can be generally described as ectopic tubule formation and migration. They are therefore very different from the well-studied *btl/FGFR* mutant phenotype, which is characterized by a lack of tubule migration (Fig. 2C). To visualize the tracheal cells, we also stained the embryos with antibody against a constituent PAS-domain transcription factor, Trachealeless (Trh; Fig. 2J). There is no detectable effect of *awd* mutations on the subcellular localization or expression level of Trh (Fig. 2K,L). In the examples shown, groups of dorsal trunk cells move ectopically (arrows in Fig. 2K,L), making a 90° turn away from the normal dorsal trunk position.

The lumen and nuclear markers documented above are useful for visualizing the tubule network and the tracheal cell positions, but they cannot provide correlation between the tubule phenotypes and the behavior of tracheal cells. To visualize the potential cellular defects in the tracheal system, the *awd^{j2A4}* allele was combined with the *1-eve-1* transgene and the embryos were stained with anti-β-Gal antibody. The β-Gal reporter protein in *1-eve-1* is expressed in both the nucleus and in cytoplasm (Fig. 1), making it the best marker for visualizing simultaneously the position and the morphology of all tracheal cells. As such, the *1-eve-1* reporter gene has been used extensively as a general tracheal marker. Nonethe-

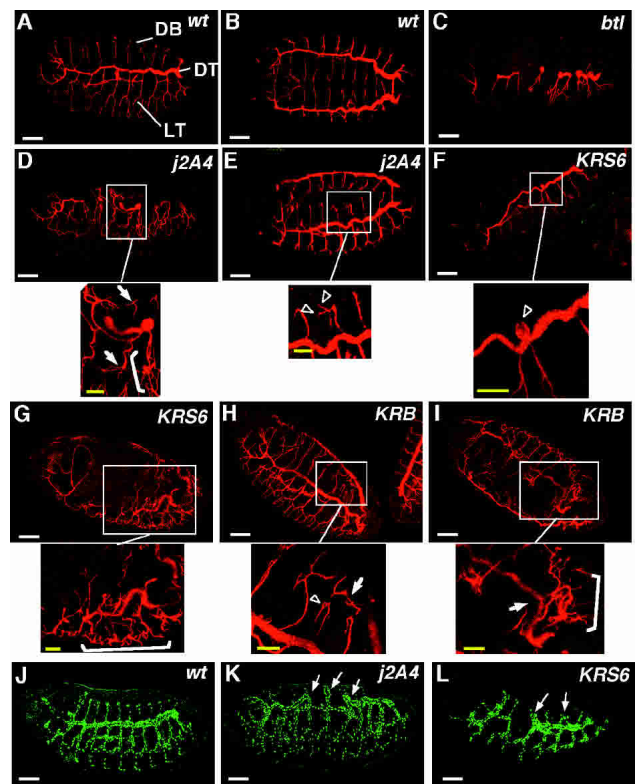


Figure 2. *awd* mutant alleles display distinct tracheal phenotypes. Embryos were collected at 25°C and double stained using the 2A12 monoclonal antibody against a lumen antigen and a FITC-conjugated polyclonal antibody against β-Gal (red) (A–I), or double stained using the rat polyclonal anti-Trh antibody (green) and mouse monoclonal anti-β-GAL antibody (J–L). *btl* and the three *awd* mutants are homozygotes (see Materials and Methods). Stage 15–16 embryos are shown with anterior to the left. (A) Lateral view of a *y, w* embryo, representing wild type. Branches relevant to the following figures are marked. (DT) Dorsal trunk; (LT) lateral trunk; (DB) dorsal branch. (B) Dorsal view of a *y, w* embryo. (C) Lateral view of a *btl* embryo. There is very little tubule formation. (D) Lateral view of an *awd^{j2A4}* embryo. There is a general disruption of the tracheal network with ectopic branches emanating from the lateral trunk (marked between arrows in the enlarged section). Also, additional branches are seen sprouting out of the lateral region (bracket). (E) Dorsal-lateral view of an *awd^{j2A4}* embryo. Two ectopic branches are shown (arrowheads). (F) Lateral view of an *awd^{KRS6}* embryo. An ectopic “bulge” is indicated (arrowhead). (G) Dorsal-lateral view of an *awd^{KRS6}* embryo. The region exhibiting abnormal branching and looping is highlighted. (H) Dorsal-lateral view of an *awd^{KRB}* embryo. One dorsal branch (DB) shows an ectopic loop (arrowhead) and two other dorsal branches form abnormal axial connection (arrow). (I) Dorsal-lateral view of an *awd^{KRB}* embryo. The region exhibits ectopic branching and looping is indicated by a bracket. Also the dorsal trunk (DT) shows an abnormal 90° turn (arrow). (J) Lateral view of a *y, w* embryo showing nuclear expression of the Trh protein in all tracheal cells. (K) Lateral view of an *awd^{j2A4}* embryo. Arrows point to dorsal trunk (DT) cells that migrate ectopically (misallocated), resulting in gaps in dorsal trunk. (L) Lateral view of an *awd^{KRS6}* embryo. Arrows point to misallocated dorsal trunk (DT) cells and ectopic connection of two dorsal branches (DB). White bars, 50 μm; yellow bars, 20 μm.

less, to ensure that it is a true “neutral” marker, we first examined a large number of *1-eve-1* embryos (homozygous viable) by anti- β -Gal staining. There are less than 1% of either *awd*-like or *btl*-like phenocopies (Fig. 3K), well within the rate of spontaneous defects. Second, the phenotypes observed in *awd^{l2A4}*, *1-eve-1* embryos can be rescued by expressing a wild-type copy of *awd* in the tracheal cells directed by the *btl* enhancer (Fig. 3K). Henceforth, *1-eve-1* will be used as a wild-type control and *awd^{l2A4}*, *1-eve-1* will be the representative *awd* allele.

The wild-type tracheal network (Fig. 3A) consists of 10 interconnected subunits on either side of the embryo. The initially stubby tubes migrate outward and are fully extended at the end of embryogenesis at stage 17 (Fig. 3B). The largest tubes connect axially and form the major trunk (dorsal trunk), while another set of tubes (dorsal branches) extends toward the dorsal midline and connects with its counterpart from the other side of the embryos (arrow in Fig. 3C). The tracheal phenotypes of the *awd* mutant, at its most severe seen mainly in ho-

mozygotes (Fig. 3D), show complete disruption of the tracheal network. Fragments of the dorsal trunks scatter throughout the embryo with random, ectopic branches sprouting out. Note that the severe disruption of the trachea observed here is probably not secondary to a general embryonic patterning defect, as other late embryonic structures such as midgut are formed properly (Fig. 3D).

The milder phenotypes seen in heterozygotes follow the same but less severe pattern. First, a segment of the dorsal trunk is “misallocated” to the position of transverse connectives (bracket in Fig. 3E), reminiscent of those observed earlier (Fig. 2I,K,L). In addition, ectopic cellular projections are seen sprouting out of these misallocated branches (insert in Fig. 3E). Second, two dorsal branches appear to fuse at the stalk, but the tips separate and connect with their counterparts across the dorsal midline (asterisk in Fig. 3F). The fusion is usually accompanied by the thickening at the base (arrowhead in Fig. 3F). We suspect that such a defect is another manifestation of misallocation of cells. In other instances, dorsal

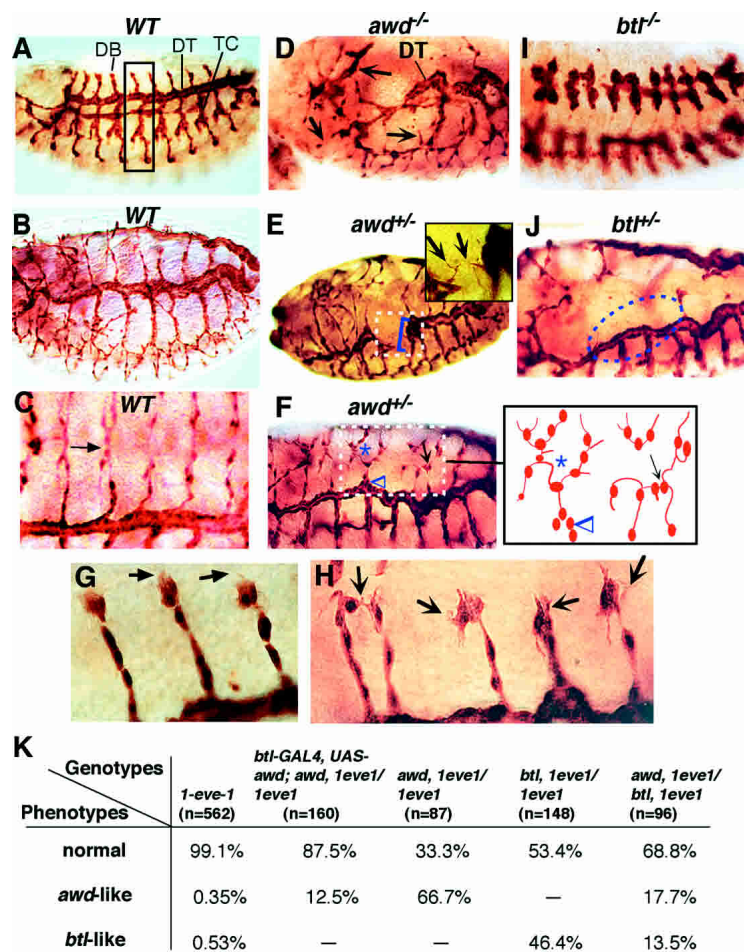


Figure 3. *awd* mutant exhibits ectopic tracheal cell migration in contrast to the *btl* phenotype. All embryos were collected at 25°C and stained with mouse monoclonal anti- β -Gal antibody. Identification of homozygous and heterozygous *awd* and *btl* is described in Materials and Methods. Unless noted, anterior is to the left and dorsal side is up. (A) Lateral view of a wild-type stage 14 embryo. One tracheal subunit is highlighted. Three tracheal branches relevant in the following figures are marked. (DB) Dorsal branches; (DT) dorsal trunk; (TC) transverse connectives. (B) Dorsal-lateral view of a wild-type stage 17 embryo showing fully extended tracheal tubes. (C) A dorsal close-up view of a wild-type stage 16 embryo showing connection of two dorsal branches across the dorsal midline (arrow). (D) Dorsal view of a stage 16 homozygous *awd^{l2A4}* embryo showing disrupted dorsal trunk (DT) and sprouts of ectopic branches (sharp arrows). The first compartment of the properly formed midgut can be seen in this view (the light, rounded internal structure in the middle). (E) Dorsal-lateral view of a stage 17 heterozygous *awd^{l2A4}* embryo. A segment of the dorsal trunk moves ventrally into the position of transverse connective (bracket) instead of connecting with the lateral neighbor. Ectopic small cellular processes are seen sprouting from the abnormal branches (sharp arrows in the insert). (F) Dorsal-lateral view of a stage 16 heterozygous *awd^{l2A4}* embryo. The highlighted region shows two dorsal branches fused at the base but separate at the tip (asterisk) as well as misconnection of two neighboring dorsal branches (sharp arrow), instead of crossing the dorsal midline. (G) Close-up view of dorsal branches of a wild-type embryo. Arrows point to the few filopodia extending from the tip cells of the dorsal branches. (H) Close-up view of dorsal branches of a heterozygous *awd^{l2A4}* embryo. Multiple, random cellular projections extend from the tip cells (sharp arrows). (I) Lateral view

of a stage 14 homozygous *btl^{H82Δ3}* embryo. There is very little tubule migration as compared to the wild type. (J) Dorsal-lateral view of a stage 16 heterozygous *btl^{H82Δ3}* embryo. The highlighted region shows lack of dorsal branch formation. (K) Quantitation of the recorded phenotypes as shown in A–J. The *awd* and *btl* alleles are *awd^{l2A4}* and *btl^{H82Δ3}*. Note that to avoid complications from early embryonic patterning defects, only embryos older than stage 13 that showed proper germband retraction and, after stage 15, proper gut formation, were tabulated. Construction of the *btl*-GAL4, UAS-*awd* rescue chromosome is described in Materials and Methods.

Dammai et al.

branches from adjacent subunits are linked, rather than connecting with the counterparts across the embryonic midline (arrow in Fig. 3F). Third, the tip cells of the dorsal branches, which receive the chemotactic signal, usually extend few stable cellular processes during the migratory phase (Fig. 3G). In *awd* heterozygotes, multiple filopodia-like projections are seen extending from the tip cells, and they often do not point toward the direction of the normal migratory path (Fig. 3H). Taken together, these phenotypes indicate that *awd* is required to regulate guided tubule cell migration. Note that we also analyzed an additional allele of *awd* (*awd*^{KRS6} in combination with *1-eve-1*) and it showed the same tracheal defect (data not shown). The *awd* mutant phenotypes shown here are again in contrast to that of *btl*. In the severe *btl* phenotype, there is very little branch migration (Fig. 3I), as noted previously (Klämbt et al. 1992; Lee et al. 1996; Dossenbach et al. 2001). In mild phenotypes, the overall tracheal network is formed but individual branches are often missing (Fig. 3J). Thus, *btl* and *awd* appear to be antagonists in regulating tracheal tube migration.

awd antagonizes *btl* and cooperates with *shi*/dynammin

The clue to the cellular defects that underlie the *awd* phenotype was provided by a recent study on the function of *Drosophila* dynammin homolog encoded by *shibire* (*shi*). Dynammin is an essential component in vesiculation by “pinching off” the invaginated vesicles from the membrane domain (reviewed in Brodin et al. 2000). In *Drosophila*, the temperature-sensitive mutants of *shi* lead to paralysis at elevated temperatures due to failure of neurotransmitter uptake through synaptic vesicle internalization at the nerve termini (Kosaka and Ikeda 1983; Delgado et al. 2000). Remarkably, in a genetic screen for mutants that exacerbate this effect, all three “enhancer” alleles isolated were *awd* mutants (Krishnan et al. 2001). It is therefore proposed that Awd, as a source of GTP, serves a guanine nucleotide exchange factor (GEF)-like function for the endocytotic activity of dynammin GTPase.

We reasoned that Shi–Awd-directed endosome formation might also function in tracheal cells for recycling and turnover of the chemotactic Btl receptor. The molecular function of dynammin has been linked to growth factor receptor internalization through endocytosis (Sever et al. 1999; reviewed in Hinshaw 2000). Furthermore, endocytosis of activated growth factor receptor is known to be essential as a first step for receptor down-regulation (Vieira et al. 1996). As such, loss of *shi* or *awd* in tracheal cells could result in overaccumulation of FGFR, leading to ectopic tracheal tube migration. If this is the case, the first prediction would be that reduced dosage of *btl* should alleviate the severity of *awd* phenotypes. As shown in Figure 3K, heterozygous mutants of these two genes each give moderate penetrance of the respective phenotypes. However, when the two mutations were combined in transheterozygotes, the *awd*-like (ectopic migration) and *btl*-like (lack of branching) phenotypes are reduced by 73% and 71%, respectively. We

have also determined that the *FGF ligand/bnl* is not over- or ectopically expressed in the *awd* mutant (Supplementary Fig. 1). Thus, the antagonist genetic interaction between *awd* and *btl* is most likely autonomous to the tracheal cells.

We next examined whether *shi* mutants would exhibit *awd*-like phenotypes. The temperature-sensitive *shi*¹ allele was used (Kitamoto 2001; Krishnan et al. 2001). Because *shi* is located on the X chromosome, we directly crossed *shi*¹ females with *1-eve-1* males. The progenies, consisting of heterozygous females and hemizygous males, were collected at permissive temperature (25°C) for 7 h and then shifted to 34°C for another 7 h. As shown in Figure 4, loss of *shi* function indeed results in ectopic migration phenotypes of differing severity. (1) A mild one with occasional ectopic branching (sharp arrow in Fig. 4A) and abnormal cellular projections from the tip cells (arrows in the insert in Fig. 4A), similar to that seen in the mild *awd* phenotypes, or (2) a more severe one characterized by misallocation of dorsal trunk cells into the position of transverse connectives (Fig. 4B), into the dorsal branch domain (Fig. 4C), or into forming an extra loop of dorsal trunk (Fig. 4D). In many cases, ectopic cellular projections can be clearly identified at the tips of ectopic branches (Fig. 4C,D). Therefore, the underlying defects in *shi* mutant appear to be similar to those in the *awd* mutant. We note that the ectopic branching (mild; Fig. 4A) and misallocation (more severe; Fig. 4B–D) of the *shi* phenotypes are approximately equal in numbers (Fig. 4G), most likely reflecting the phenotypic outcomes of heterozygous females and the hemizygous males, respectively.

The endocytosis model proposed above also predicted that *awd* and *shi* mutants would mutually exacerbate their phenotypic outcomes. This proved to be true. *awd* and *shi* transheterozygotes (or heterozygote–hemizygote combinations) show high phenocopy numbers of total disruption of the tracheal network, with breakaway branches and tracheal cells (Fig. 4E). Note that in the example shown in Figure 4E, the underlying internal structures such as midgut are formed properly (data not shown), indicating that the tracheal phenotype is not due to a general disruption of embryonic pattern formation. These extremely severe phenotypes resemble those observed in the most severe *awd* homozygous mutants and were observed very rarely in conditional *shi* hetero- or hemizygotes (Fig. 4F). Also, these severe defects were not seen when *awd* heterozygotes were shifted to elevated temperatures (data not shown), indicating that the resulting tracheal phenotypes are specific for *awd*–*shi* interaction and not due to effects of elevated temperatures on *awd* heterozygosity.

FGFR is overexpressed in *awd* mutant

Having established that *awd* and *shi* cooperate in guided tracheal cell migration, we next asked whether in *awd* mutant the FGFR was overexpressed, as the proposed endocytotic function of *shi*–*awd* would predict. A *btl*-*GFP* chimeric transgene (Sato and Kornberg 2002) was expressed under the control of cognate *btl* promoter (see

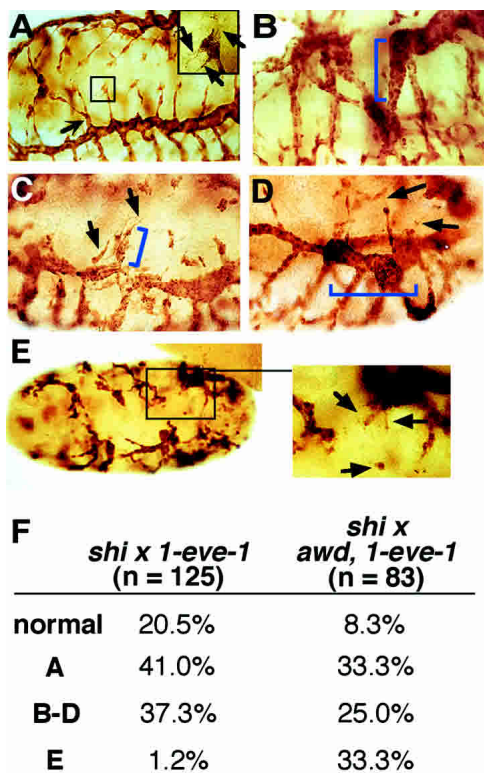


Figure 4. *shi* mutant shows migration phenotype similar to *awd*. Progenies of *shi*¹ homozygous females crossed with *1-eve-1* males (A–D) and of *shi*¹ homozygous females crossed with *1-eve-1, awd*^{12A4/TM3, P[ry + t7.2 = HZ2.7]DB2, Sb males (E). The embryos were collected at 25°C for 7 h, then incubated for 7 h at 34°C and stained with anti-β-Gal antibody. Unless indicated, anterior is to the left and dorsal side is up. (A) Dorsal-lateral view. A sharp arrow points to the ectopic branching event. Also, abnormal cellular projections are seen extending from the dorsal branch tip cells (arrows in the inset). (B) Lateral view. A segment of the dorsal trunk is seen moving ventrally (bracket) into the position normally occupied by transverse connectives, instead of anteriorly to connect with the lateral neighbor. (C) Dorsal-lateral view. A group of tracheal cells move dorsally (bracket) at the expense of forming a proper dorsal trunk connection. Ectopic cellular extensions are also visible (arrow). (D) Lateral view. An extra loop of dorsal trunk is formed (bracket) with ectopic small projections (arrows). (E) Dorsal view of severely disrupted trachea. The enlarged section shows ectopic cellular projections and randomly migrating tracheal cells (arrows). (F) Quantitation of the recorded phenotypes as shown in A–E. There is a nearly 30-fold increase in the most severe phenotype (E) when *shi* is combined with heterozygous *awd* mutant. Only embryos older than stage 13 that appear normal in segmental patterns were tabulated as described in Figure 3K.}

Materials and Methods). In the wild-type genetic background, the Btl-GFP fusion protein is barely detectable in the tracheal cells (Fig. 5A), showing that expression of Btl-GFP by itself does not lead to overaccumulation of the fusion protein. This indicates that the expression level of *btl-GFP* is likely under the same stringent feedback control as for the endogenous *btl* (Ohshiro and Saigo 1997). Significantly, at high magnification Btl-

GFP-containing particles are seen internalized in all tracheal cells of wild-type embryo (Fig. 5A–C), consistent with the notion that active internalization from the membrane domain prevents surface accumulation of Btl-GFP. This is further exemplified by lack of tracheal abnormality in wild-type embryos expressing Btl-GFP. However, in *awd* mutant, Btl-GFP accumulates at very high levels in the periphery of all tracheal cells. Such accumulation can be seen in mild dorsal branch fusion (Fig. 5D), in abnormal tubule migration involving multiple dorsal branches (Fig. 5E), or in ectopic branches emanating from severely disrupted tracheal network (Fig. 5F). At higher magnification, Btl-GFP is seen outlining very small cellular processes (Fig. 5E). Also, large aggregates of Btl-GFP are observed only in *awd* mutant background (Fig. 5D,E). Overaccumulation of Btl-GFP is confirmed by Western blot quantitation (Fig. 5G). It is worth noting that the in vivo Btl-GFP is detected as a smear at the molecular weight of ~150 kD (Btl120 + GFP26 kD), indicating extensive posttranslational modifications. In addition, the overaccumulation effect is somewhat specific, as the level of EGF receptor (EGFR) is not increased. Also note that the *shi-awd*-directed turnover of FGFR is a function of all tracheal cells, that is, not dependent on ligand binding, as the overaccumulation is not restricted to tracheal tip cells in proximity to the presumed source of FGF ligand (Fig. 5E). We find that the *btl-GFP* chimeric gene is most likely functional in vivo because this transgene exacerbates the otherwise mild expressivity of the *awd* heterozygotes, resulting in significantly increased severe tracheal defects (~20%; see Fig. 5F for an example). As mentioned previously, these very severe phenotypes are rare in the *awd* heterozygote alone and not seen in wild-type embryos upon Btl-GFP expression. Thus, the accumulation of Btl-GFP in tracheal cells and the phenotypic outcome of this accumulation correlate specifically with the loss of *awd* function.

Significantly, the *awd* mutant effect on FGFR accumulation can be duplicated in the cultured cells. When the overall Awd protein levels are knocked down by RNA interference (RNAi; Fig. 6A), the overall FGFR levels increased dramatically (Fig. 6B). When visualized by staining for GFP, the cells examined before the RNAi took effect showed only low-level, internalized signal (Fig. 6C,D). When the Awd level was knocked down, a substantial number of the cells overaccumulate the Btl-GFP chimeric protein on the cell surface (Fig. 6E,F). Most remarkably, these Btl-GFP overexpressing cells extend either multiple filopodia (microspikes) or lamellipodia. It is also worth noting that *awd* knock-down does not affect the levels of EGF receptor (EGFR; Fig. 6B), indicating that intracellular transport and turnover mechanism for EGFR and FGFR are likely different.

MAPK is ectopically activated in awd mutant trachea

Although the signaling events downstream of Btl are likely very complex, leading to cellular responses that alter gene expression and cytoskeletal structures, one accessible indicator is the activation of MAP kinase

Dammai et al.

Figure 5. Overaccumulation of Btl/FGFR in *awd* mutant. The genotypes of the indicated embryos are *y, w; btl-GAL4/+; 1-eve-1, UAS-btl-GFP/+* (wt) and *y, w; btl-GAL4/+; 1-eve-1, UAS-btl-GFP, awd^{12A2}/+* (*awd/+*). Embryos were double stained with anti- β -Gal (red) and anti-GFP (green) antibodies. The two channels were recorded sequentially. Anterior is to the left. (A) Dorsal-lateral view of a wild-type stage 14 embryo. A projection of five 2- μ m confocal sections. The Btl-GFP chimeric protein is barely detectable. In the close-up image (single confocal section), circles mark individual tracheal cells and sharp arrows point to examples of internalized Btl-GFP. (B) Lateral view of portion of a wild-type stage 12 tracheal subunit. Circles mark individual tracheal cells and sharp arrows point to examples of internalized Btl-GFP. Single confocal section. (C) Single confocal section of a wild-type stage 15 dorsal branch tip cell. Sharp arrows point to examples of internalized Btl-GFP. (D) Stage 13 *awd/+* tracheal subunits. A projection of five 1- μ m confocal sections. In the close-up image, arrows point to examples of large aggregates of Btl-GFP. (E) Lateral view of three dorsal branches from a stage 15 *awd/+* embryo. A projection of five 1- μ m confocal sections. Abnormal migration (sharp arrows), ectopic cellular projections (asterisk), and high level of Btl-GFP are seen. In the close-up images (single confocal section), Btl-GFP is seen outlining a very fine cellular projection (bracket). Note that the close-up section is only partially included in the projected image. (F) Dorsal view of a stage 17 *awd/+* embryo. A projection of five 2- μ m confocal sections. The total disruption of the tracheal system is rarely seen in the *awd* heterozygotes. The properly formed midgut can also be seen beneath the abnormal tracheal branches (red auto-fluorescence). The enlarged view (GFP stain only) shows high level of Btl-GFP expression and ectopic cellular projections (arrows). (G) Western blot quantitation of the Btl-GFP accumulation. Embryonic extracts from *awd/+* and *wt* embryos as described above were Western blotted and probed with antibodies indicated. Two independent lines of *1-eve-1, UAS-btl-GFP, awd^{12A4}* were examined. Because the *btl-GFP* and the *1-eve-1* transgenes are located on the same chromosome, β -Gal was used as a loading control. Btl-GFP is up-regulated by approximately fivefold whereas there is no concomitant increase in EGFR (a slight decrease, in fact) or the total MAPK levels in the *awd* mutant.

(MAPK). The Btl pathway is known to be the sole contributor for MAPK activation in tracheal cells from stage 11 onwards, when the cells just begin to migrate from the tracheal placodes towards the source of Bnl. For example, the extracellular domain of Btl, when fused to the C-terminal tyrosine kinase domains of other RTKs, is sufficient to activate MAPK and rescues tracheal phenotypes in *btl* mutants (Dossenbach et al. 2001). In Figure 7 we show the MAPK activation pattern at stages 12 and 15 when there is active branch migration. Note that after stage 12 there is no more EGFR-directed signaling that specifies tracheal cell fates along the anteroposterior axis (Wappner et al. 1997). The activated MAPK is detected using an antibody against a dually phosphorylated 11-amino-acid peptide encompassing the ERK1/2 activation site (designated dp-MAPK; Gabay et al. 1997; Yao et al. 2000). In wild-type stage 12 trachea, the activated MAPK is detected in some, but not all, of the migrating tips (Fig. 7A) in agreement with the dynamic pattern of MAPK activation documented by previous studies (Dammai and Hsu 2003). In wild-type stage 15 trachea, activated MAPK is detected exclusively in one migrating tip cell

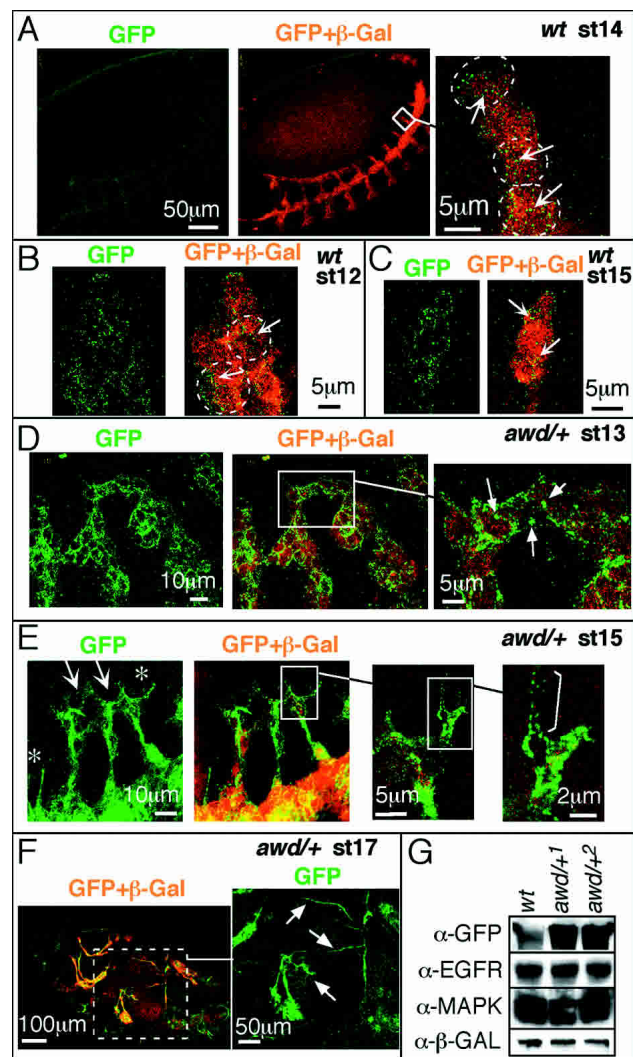


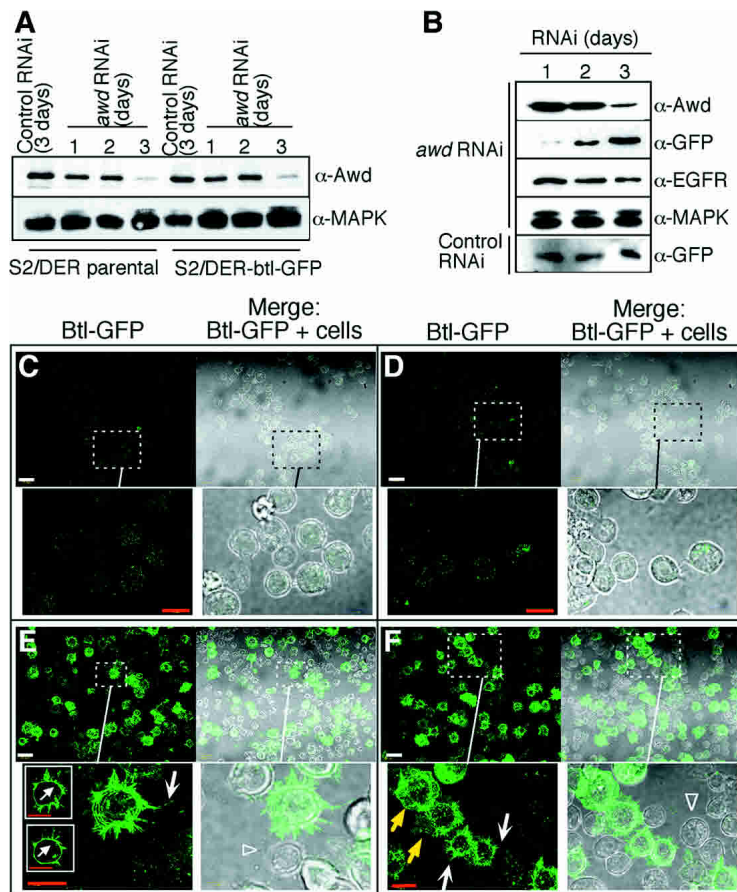
(Fig. 7B). In *awd* mutant at stage 12, by contrast, activated MAPK is detected in multiple cells within the tracheal placodes (Fig. 7C), whereas at stage 15 activated MAPK is detected throughout the abnormally fused dorsal branches, including the stalk cells (Fig. 7D).

Discussion

We explored the mechanism of *awd*, the *Drosophila* homolog of the putative metastasis inhibitor *nm23*, in cell migration events during tracheal tube formation. The *awd* mutant phenotype does not resemble defects in other pathways that are known to be involved in promoting tracheal development, but are more consistent with loss of direction and increased motility of the tracheal cells due to hyperactivity of pathways involving FGFR.

awd cooperates with shi/dynammin to down-regulate the Btl/FGFR levels

Earlier studies established that *awd* participates in synaptic vesicle internalization likely by supplying GTP-re-



overexpressing cells extend multiple filopodia (microspikes; white sharp arrows) or lamellipodia (block yellow arrow), whereas nonoverexpressing cells remain rounded with no or very few protrusions (open arrowhead). The insets in *E* are single confocal sections, showing the localization of overexpressed Btl-GFP in the cell membrane. White bars, 20 μm ; red bars, 10 μm .

quired for Shi/dynamin-mediated endocytosis (Krishnan et al. 2001). Our data strongly support the model in which Shi/dynamin and Awd/Nm23 are also recruited to modulate RTK signaling through endocytosis of Btl/FGFR. First, the *awd* tracheal phenotype (Figs. 2, 3) is alleviated by reducing the dosage of *btl*, indicating that *awd* may normally down-regulate the *btl* expression level (Fig. 3K). Second, this assertion is supported by direct demonstration of overaccumulated Btl-GFP chimeric protein in the *awd* mutant background (Fig. 5D–F). Third, *shi* mutant phenotypes resemble those in the *awd* mutants (Fig. 4A–D). In addition, *awd* and *shi* cooperate in the same pathway, as heterozygous *awd* combined with *shi* heterozygotes or hemizygotes exhibit exaggerated phenotypes that are much more severe compared to *awd* or *shi* alone (Fig. 4E,F). Fourth, using a *btl-GFP* chimeric transgene controlled by the cognate *btl* promoter, we observed FGFR internalization in the wild-type trachea (Fig. 5A–C). Finally, we show that one prominent downstream effector of the FGFR signaling, MAPK, is ectopically activated in multiple tracheal cells that normally do not experience Bnl signaling (Fig. 7). These results, coupled with our observation that *bnl* expression pattern in the stroma is not altered in *awd* mutant

Figure 6. *awd* knock-down in S2 cells generates phenotypes reminiscent of those in the *awd* trachea. Unless specified, all confocal images are projection of five 1- μm sections. (A) S2 cells stably expressing *Drosophila* EGFR (S2/DER; Schnepf et al. 1998) were cotransfected with either *awd*-specific duplex RNA (*awd* RNAi) or duplex RNA corresponding to the pBlueScript multicloning sites (control RNAi), and with pUC-HygMT vector or with pUC-HygMT-btl-GFP (S2/DER parental or S2/DER-btl-GFP, respectively). Cells were then treated with CuCl_2 for inducing the metallothionein (MT) promoter. Cell extracts collected at the indicated time after transfection were Western blotted and probed with anti-Awd antibody and reprobbed with antibody against total MAPK, which serves as a loading control. Significant reduction of the Awd protein levels was observed 3 d after RNAi treatment in both cell types, indicating the *btl-GFP* transgene has no effect on Awd expression. The reduction is not due to cell death, as no obvious decrease of cell numbers was noted. Also, the cells appeared to be healthy (see below). (B) S2/DER cells were transfected with RNA duplex and pUC-HygMT-btl-GFP as in A. Cell extracts were prepared at 1, 2, and 3 d after transfection and Western blotted with the indicated antibodies. There is a significant increase in the GFP levels in step with the decrease in the Awd levels. By contrast, reduction of Awd has only a slight negative effect on the EGFR levels. (C,D) Two fields of the S2/DER-btl-GFP treated above at 2 d after transfection, when no significant Awd reduction was observed. Low levels of Btl-GFP are mostly internalized. (E,F) Two fields of the S2/DER-btl-GFP treated above at 3 d after transfection, when significant Awd reduction was observed. A large number of cells shows overaccumulation of Btl-GFP in the cell periphery. These Btl-GFP

(Supplementary Fig. 1), indicate that internalization of membrane-bound FGFR, mediated by *awd* and *shi/dynamin*, plays a major role in ensuring the proper level of chemotactic signal response in the tracheal cells. This notion is further supported by the observation in cultured cells, in which overaccumulation leads to dramatic formation of microspikes and lamellipodia (Fig. 6).

It has been well established that excessive cell surface receptor density can lead to ligand-independent activation of downstream pathways by lateral aggregation and propagation of receptor phosphorylation (Verveer et al. 2000; Sawano et al. 2002). Indeed, it has been shown that forced dimerization of the Btl protein devoid of the ligand-binding domain can induce ectopic migration phenotypes similar to those observed in *awd* and *shi* (Lee et al. 1996).

Are there other potential targets of Awd–Shi action in tracheal development?

In developing *Drosophila* eye and wing imaginal discs, the extracellular domain (ECD) of the membrane-associated Notch is cleaved upon binding to the membrane-bound ligand Delta on the neighboring cell. The Delta–

Dammai et al.

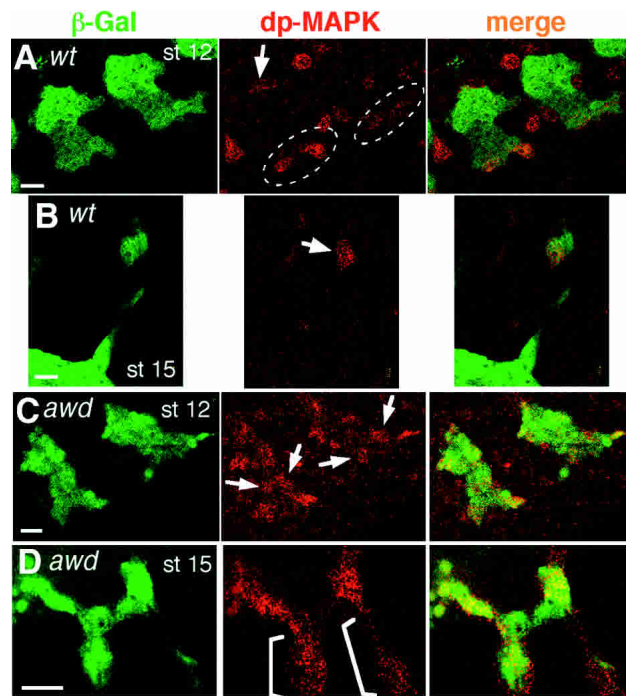


Figure 7. Ectopic activation of MAPK in *awd* mutant. *1-eve-1* (*wt*) and *awd^{12A4}, 1-eve-1/1-eve-1* (*awd/+*) stage 12 and stage 15 embryos were double stained with anti- β -Gal-FITC (green) and anti-dp-MAPK (red) antibodies. The two channels were recorded sequentially. Anterior is to the left. (A) Tracheal subunits of a stage 12 wild-type embryo. A projection of five 1.5- μ m confocal sections. Within the tracheal placodes, activated MAPK are detected in the two tips cells marked by circles. Lighter MAPK activation is also detected on the opposite tip (arrow). Activated MAPK-expressing cells surrounding the tracheal placodes are of mesodermal origin, including cardiac precursors. (B) One dorsal branch of a wild-type stage 15 embryo. A single confocal section. Only one cell at the tip contains activated MAPK. (C) Tracheal subunits of a stage 12 *awd* heterozygote. A projection of five 1.5- μ m confocal sections. Multiple cells besides the migrating tips within the tracheal placodes express activated MAPK (arrows). (D) Two laterally fused dorsal branches of a stage 15 *awd* heterozygote. A projection of five 1.5- μ m confocal sections. The stalks (brackets) ectopically express activated MAPK. Bars, 10 μ m.

Notch^{ECD} complex is then internalized by endocytosis into the Delta-expressing cell. Removal of Notch^{ECD} facilitates the activation and dissociation of the Notch intracellular domain from the membrane by proteolytic cleavages. Interestingly, reduction of endocytosis due to *shi* mutation leads to reduced Notch signaling (Parks et al. 2000). In tracheal cells, Notch expression in one of the two tip cells suppresses the fusion cell fate whereas the other cell (Delta-expressing) goes on to fuse with its opposing partner on the other branch (Ikeya and Hayashi 1999; Llimargas 1999; Steneberg et al. 1999). In *Notch* loss-of-function mutant, additional fusion cells are generated and misconnection between neighboring tubes can be observed. Such a defect is also observed in *awd* mutants. However, in *awd* mutants, the most prominent defects are the result of misguided migration of tracheal

tubes and individual tracheal cells, which are not observed in *Notch* mutant. We also argue that lateral fusion requires not only ectopic fusion cell fate but also misdirected migration. It has been suggested that Btl and Notch signaling can negatively modulate each other in the tip cells (Ikeya and Hayashi 1999). Thus, the misconnection and lateral fusion observed could be due to downstream events of hyperactive FGFR signaling. Indeed, we observed only reduction, not overaccumulation, of either Delta or N^{ecd} in the fusion cells in *awd* mutant (Supplementary Fig. 2; data not shown).

Shi is also implicated in retrieval of Spitz (an EGFR ligand) and Sog (a Dpp antagonist) such that the spatial distribution and half-life of these extracellular ligands are restricted (Lee et al. 2001; Srinivasan et al. 2002). Although EGFR and Dpp signaling pathways are involved in tracheal cell fate determination (Wappner et al. 1997), they do not participate in guided cell migration.

Another potentially relevant target of endocytosis is E-cadherin. Recently, it was shown that ARF-6 (ADP-Ribosylation Factor) recruits Nm23H1 to mediate adherens junction disassembly, indicating that Nm23H1 is involved in turnover of the transmembrane protein E-cadherin (Palacios et al. 2002). However, in *Drosophila* trachea, E-cadherin is specifically required for fusion of two opposing branches (Tanaka-Matakatsu et al. 1996). Potential lack of E-cadherin internalization therefore cannot account for the misguided migration phenotypes observed in *awd* and *shi* mutants.

We did, however, note that *Awd* is not a general regulator of RTK expression. In embryos as well in cultured S2 cells, the EGFR levels are not affected by *awd* mutation or down-regulation (Figs. 5G, 6B). What confers the specificity warrants further investigation.

The antimetastatic function of awd/nm23

Because *awd/nm23* encodes a NDPK, it is believed that *Awd/Nm23* may act as a GEF-like activator of GTPases. However, no definitive target GTPases have been identified for human Nm23 that can fully account for its antimetastatic activity. In light of the recent finding that FGF signaling is one of the very few "signature events" that underlie the metastatic potential of breast cancer (Kang et al. 2003), our demonstration that *awd/nm23* modulates cell migration via its participation in FGFR signaling provides one plausible mechanism for its antimetastatic function.

We have observed that neither the expression level nor the subcellular localization of Shi/dynamin was altered in *awd/nm23* mutants (V. Dammai and T. Hsu, unpubl.). It was also observed that *Awd/Nm23* and Shi/dynamin did not form a stable complex in vivo (Krishnan et al. 2001; V. Dammai and T. Hsu, unpubl.). Thus, *Awd/Nm23* likely supplies GTP through additional bridging factors (e.g., ARF-6; see above) or by increasing the local GTP concentration.

As we have noted in this report, *awd* mutant does not grossly affect the embryonic development. The *awd* mutant was originally described as early pupal lethal (Biggs

et al. 1988; Dearolf et al. 1988), although the embryonic viability may simply be the result of maternal contribution of *awd*. In addition, embryos and larvae can tolerate quite well minor tracheal defects described in this report (Guillemin et al. 1996; V. Dammai and T. Hsu, unpubl.). Why, then, is the *awd* mutant effect limited if *awd* is involved in regulating such important cellular process as endocytosis? Our data showing the differential effects of *awd* mutant on FGFR and EGFR strongly suggest that Awd, unlike Shi/dynamin, is not a general regulator of endocytosis. Dynamin has been shown to regulate vesicle formation from various membrane domains, not restricted to the cell surface (reviewed in Hinshaw 2000). As such, Awd may selectively regulate a subset of vesicle transport events, perhaps depending on the availability of the cofactors or the "bridging factors" described above.

Materials and methods

Drosophila strains and genetics

The *awd*^{12A4} allele is a single P-element insertion, resulting in complete null genotype. It has been characterized (Krishnan et al. 2001) and the insertion site has been mapped to the 5' untranslated region by the *Drosophila* genome project (Spradling et al. 1999). *y; Df(3R)awd*^{KRB}, *e, ca*¹/*TM3, Sb, Ser* is a small chromosomal deficiency uncovering 100D1–100D3–4. *y; awd*^{KRS6}/*y⁺, TM3, Sb, Ser* was a gift from A. Shearn (Johns Hopkins University, Baltimore, MA). The *shi*¹ is a temperature-sensitive allele that has been described extensively (see the FlyBase Web site for a complete list of reference: <http://flybase.bio.indiana.edu/bin/fbidq.html?FBal0015610>). The *btl*^{H82Δ3} allele, a hypomorph, is partial deletion of the *btl* 5' regulatory region (Klämbt et al. 1992). The *awd*^{12A4}, *awd*^{KRB}, and *shi*¹ strains are obtained from the Bloomington *Drosophila* Stock Center and the *btl*^{H82Δ3} strain is a gift from D. Montell (Johns Hopkins University, Baltimore, MA). The transgenic line *1-eve-1* (a gift from A. Brand, University of Cambridge, Cambridge, UK) contains the *lacZ* reporter gene under control of the *trachealless* gene promoter that specifies expression in all tracheal cells at all stages. The *1-eve-1* marker was combined with either *awd*^{12A4} or *btl*^{H82Δ3} allele (all three on the third chromosome) by simple genetic recombination. All *awd* and *btl* alleles were paired with the balancer chromosome containing another reporter *lacZ* line that specifies β-Gal expression in the maxillary segment (*TM3, P{ry + t7.2 = HZ2.7}DB2, Sb*; from the Bloomington Stock Center). Therefore, when embryos resulting from heterozygous intercross were stained with anti-β-Gal antibody, expression in only tracheal cells and not in the anterior embryonic segments indicates homozygosity. The heterozygous mutants were the result of *1-eve-1, awd*^{12A4} (or *btl*^{H82Δ3})/*TM3, P{ry + t7.2 = HZ2.7}DB2, Sb* crossed with homozygous *1-eve-1*, to avoid complication from the mutations on the balancer chromosome. In this case, no maxillary staining indicates heterozygosity.

The *btl-GAL4* and *UAS-btl-GFP* transgenic lines are gifts from T. Kornberg (University of California, San Francisco) and have been described (Sato and Kornberg 2002). The *UAS-btl-GFP* marker was combined with *1-eve-1, awd*^{12A4}. The *1-eve-1, UAS-btl-GFP, awd*^{12A4}/*TM3, P{ry + t7.2 = HZ2.7}DB2, Sb* was then crossed with *btl-GAL4* homozygotes to induce *btl-GFP* expression. Thus, only those embryos stained with β-Gal in the trachea are relevant.

For analysis of *shi* phenotypes, homozygous *shi*¹ (on the X chromosome) females were crossed with homozygous *1-eve-1* males. The resulting embryos were therefore either heterozygous females or hemizygous males, and all were stained by anti-β-Gal in trachea. Because *shi*¹ allele is temperature sensitive, embryos were collected continuously at the permissive temperature (25°C) for 7 h, that is, a collection of embryos encompassing stages 1–11. The embryos were then removed from egg-laying flies and incubated at restrictive temperature (34°C) for another 7 h. Thus the final collection of embryos was about stages 11–16, an approximation due to growth variations at high temperature. For *shi-awd* interaction, homozygous *shi*¹ females were crossed with *1-eve-1, awd*^{12A4}/*TM3, P{ry + t7.2 = HZ2.7}DB2, Sb*.

To generate the *awd* transgenic strain, the wild-type *awd* open reading frame was cloned into the P-element transformation vector pUAST, downstream from the yeast UAS enhancer element. The resulting DNA was injected into the *y, w* embryos and transgenic animals isolated using the established methodology. Transgenics (two independent strains) carrying the transgene on the second chromosome were combined with the *btl-GAL4* (on the second chromosome; see above). The resulting *y, w; btl-GAL4, UAS-awd* (homozygous viable) was used to rescue the phenotypes of the *awd* alleles (see text).

Antibodies

Bacterially expressed, His-tagged Awd protein was purified using Ni-NTA column (Qiagen) and the antibody raised in rabbits. Rabbit polyclonal antibody was affinity purified using protein A-agarose beads (Bio-Rad). The final IgG concentration was 2.95 mg/mL. A 1:1000 dilution was used for fluorescence staining and 1:2500 was used for Western blotting. Mouse monoclonal anti-β-Gal antibody (Sigma) was used at 1:1500 (overnight incubation at 4°C) for colorimetric staining and 1:500 for confluorescence staining with anti-Awd antibodies. Rabbit polyclonal anti-β-Gal-FITC conjugate (Rockland; at 1:500) was used for fluorescence costaining with anti-dp-MAPK. Rabbit polyclonal anti-ERK1/2 (from Sigma) was used at 1:1000 for Western. Goat polyclonal anti-*Drosophila* EGFR (from Santa Cruz Biotechnology) was used at 1:500 for Western. Mouse monoclonal antibody against dually phosphorylated (dp-) MAPK (Sigma) was used at 1:300 dilution for overnight incubation at 4°C. Rabbit polyclonal anti-GFP was used at 1:200 dilution for overnight incubation at 4°C and 1:1000 for Westerns (from AbCam and Stressgene, respectively). For fluorescence staining, Mouse monoclonal 2A12 was from Developmental Studies Hybridoma Bank (DSHB) and used at a 1:3 dilution. Mouse monoclonal anti-Delta and anti-N^{ecd} antibodies were from DSHB and used at a 1:200 dilution. Rat polyclonal anti-Trh antibody was a gift from B.-Z. Shilo (Weizmann Institute, Rehovot, Israel) and used at a 1:1000 dilution. Alexafluor 488- or 546-conjugated secondary antibodies were used (Molecular Probes) at a 1:200 dilution in a 2-h incubation at room temperature. For color staining, biotin-conjugated secondary antibodies (Vector) were used at a 1:1000 dilution in a 2-h incubation at room temperature. Color development used the VectaStain reagents following the manufacturer's instructions (Vector).

Western blotting and immunohistochemistry

For Western blotting, embryos were collected, dechorionated in 50% bleach (Clorox) and immediately sonicated in RIPA buffer with protease inhibitors (Roche). S2 cell extracts were prepared as described before (Hsu et al. 2001). One hundred micrograms of total extracts were then subjected to 10%–15%–20% step-

Dammai et al.

gradient SDS-PAGE. Blotting and protein detection followed standard procedures (Hsu et al. 2001).

For immunostaining of embryos, the embryos were dechorionated, fixed for 10 min in 0.1 M HEPES (pH 6.9)/20 mM MgSO₄ containing 4% paraformaldehyde overlaid with heptane. After fixation, the embryos were recovered with methanol. Immunostaining was performed as described (Sato and Kornberg 2002). The use of antibodies was described above.

S2 cell culture assays

S2 cell line stably expressing *Drosophila* EGFR (S2/DER) is a gift from A. Simcox (Ohio State University). The DNA sequence encoding the Btl-GFP chimeric protein was released from the *UAS-btl-GFP* construct (a gift from Makoto Sato of the University of Tokyo, Tokyo, Japan) and recloned into the *pUC-HygMT* expression vector (a gift from C. Thummel, the University of Utah, Salt Lake City, Utah) downstream from the metallothionein promoter. Duplex RNAs were generated as follows: The *pBS-awd* cDNA clone containing the *awd* coding sequence was PCR amplified using T7- and T3-promoter sequence primers. The DNA fragment was then used for synthesizing RNAs from either T7 promoter or T3 promoter using reagents supplied by Promega. The two complementary RNA strands were heat denatured at 80°C and annealed at 37°C in 1× TE (10 mM Tris-HCL at pH 7/1 mM Na-EDTA). Double-stranded RNA was gel purified. Control RNA duplex synthesis followed the same procedure except that the empty pBS vector was used.

Two micrograms of *pUC-HygMT-btl-GFP* was cotransfected with 4 µg of either control RNAi or *awd* full-length duplex RNA in 6-well plates with 1 mL of serum-free M3 media (from GIBCO). After 12 h, the transfection mixture was aspirated and prewarmed complete media was added. The cells were allowed to recover for 12 h. Ten micromolar CuCl₂ was added and samples were collected at 24, 48, and 72 h post-CuCl₂ treatment. For immunostaining, cells were identically treated as above except that the cells were grown on poly-lysine-treated coverslips and processed for immunohistochemistry as described (Mantrova and Hsu 1998).

RNA in situ and immunohistochemistry double staining

The procedures followed the published protocol (Manoukian and Krause 1992). The *btl* RNA probe corresponds to the N terminus of the open reading frame (713 nt).

Acknowledgments

We wish to thank A. Brand, T. Kornberg, D. Montell, and A. Shearn for gifts of fly strains; A. Simcox for the S2/DER cells; M. Sato for the btl-GFP cDNA; and B.-Z. Shilo for the Trh antibody. The Bloomington *Drosophila* Stock Center is also indispensable for providing critical fly stocks. J. Ivey's management of the fly facility at MUSC is greatly appreciated. This work is supported by grants from the NCI (CA095888), NIH (RO1GM57843), and VHL Family Alliance to T.H.; an Abney Foundation Fellowship to K.R.L.; and a grant from Lutz-E.-Adolf-Foundation to B.A.

The publication costs of this article were defrayed in part by payment of page charges. This article must therefore be hereby marked "advertisement" in accordance with 18 USC section 1734 solely to indicate this fact.

References

Aravind, L. and Koonin, E.V. 1998. A novel family of predicted phosphoesterases includes *Drosophila* prune protein and bacterial RecJ exonuclease. *Trends Biochem. Sci.* **23**: 17–19.

- Biggs, J., Tripoulas, N., Hersperger, E., Dearolf, C., and Shearn, A. 1988. Analysis of the lethal interaction between the prune and Killer of prune mutations of *Drosophila*. *Genes & Dev.* **2**: 1333–1343.
- Biggs, J., Hersperger, E., Steeg, P.S., Liotta, L.A., and Shearn, A. 1990. A *Drosophila* gene that is homologous to a mammalian gene associated with tumor metastasis codes for a nucleoside diphosphate kinase. *Cell* **63**: 933–940.
- Brodin, L., Low, P., and Shupliakov, O. 2000. Sequential steps in clathrin-mediated synaptic vesicle endocytosis. *Curr. Opin. Neurobiol.* **10**: 312–320.
- Dammai, V. and Hsu, T. 2003. EGF-dependent and independent activation of MAP kinase during *Drosophila* oogenesis. *Anat. Rec.* (in press).
- Dearolf, C.R., Hersperger, E., and Shearn, A. 1988. Developmental consequences of *awd*^{bs}, a cell-autonomous lethal mutation of *Drosophila* induced by hybrid dysgenesis. *Dev. Biol.* **129**: 159–168.
- Delgado, R., Maureira, C., Oliva, C., Kidokoro, Y., and Labarca, P. 2000. Size of vesicle pools, rates of mobilization, and recycling at neuromuscular synapses of a *Drosophila* mutant, *shibire*. *Neuron* **28**: 941–953.
- Dossenbach, C., Rock, S., and Affolter, M. 2001. Specificity of FGF signaling in cell migration in *Drosophila*. *Development* **128**: 4563–4572.
- Fan, Z., Beresford, P.J., Oh, D.Y., Zhang, D., and Lieberman, J. 2003. Tumor suppressor NM23-H1 is a granzyme A-activated DNase during CTL-mediated apoptosis, and the nucleosome assembly protein SET is its inhibitor. *Cell* **112**: 659–672.
- Freije, J.M., Blay, P., MacDonald, N.J., Manrow, R.E., and Steeg, P.S. 1997. Site-directed mutation of Nm23-H1. Mutations lacking motility suppressive capacity upon transfection are deficient in histidine-dependent protein phosphotransferase pathways in vitro. *J. Biol. Chem.* **272**: 5525–5532.
- Gabay, L., Seger, R., and Shilo, B.Z. 1997. MAP kinase in situ activation atlas during *Drosophila* embryogenesis. *Development* **124**: 3535–3541.
- Glazer, L. and Shilo, B.Z. 1991. The *Drosophila* FGF-R homolog is expressed in the embryonic tracheal system and appears to be required for directed tracheal cell extension. *Genes & Dev.* **5**: 697–705.
- Guillemin, K., Groppe, J., Ducker, K., Treisman, R., Hafen, E., Affolter, M., and Krasnow, M.A. 1996. The pruned gene encodes the *Drosophila* serum response factor and regulates cytoplasmic outgrowth during terminal branching of the tracheal system. *Development* **122**: 1353–1362.
- Hinshaw, J.E. 2000. Dynamin and its role in membrane fission. *Ann. Rev. Cell Dev. Biol.* **16**: 483–519.
- Hsu, T., McRackan, D., Vincent, T.S., and de Couet, H. G. 2001. *Drosophila* Pin1 prolyl isomerase Dodo is a MAP kinase signal responder during oogenesis. *Nat. Cell Biol.* **3**: 538–543.
- Ikeya, T. and Hayashi, S. 1999. Interplay of Notch and FGF signaling restricts cell fate and MAPK activation in the *Drosophila* trachea. *Development* **126**: 4455–4463.
- Kang, Y., Siegel, P.M., Shu, W., Drobnjak, M., Kakonen, S.M., Cordon-Cardo, C., Guise, T.A., and Massague, J. 2003. A multigenic program mediating breast cancer metastasis to bone. *Cancer Cell* **3**: 537–549.
- Kantor, J.D., McCormick, B., Steeg, P.S., and Zetter, B.R. 1993. Inhibition of cell motility after nm23 transfection of human and murine tumor cells. *Cancer Res.* **53**: 1971–1973.
- Kitamoto, T. 2001. Conditional modification of behavior in *Drosophila* by targeted expression of a temperature-sensitive *shibire* allele in defined neurons. *J. Neurobiol.* **47**: 81–92.

- Klämbt, C., Glazer, L., and Shilo, B.Z. 1992. *breathless*, a *Drosophila* FGF receptor homolog, is essential for migration of tracheal and specific midline glial cells. *Genes & Dev.* **6**: 1668–1678.
- Kosaka, T. and Ikeda, K. 1983. Possible temperature-dependent blockage of synaptic vesicle recycling induced by a single gene mutation in *Drosophila*. *J. Neurobiol.* **14**: 207–225.
- Krishnan, K.S., Rikhy, R., Rao, S., Shivalkar, M., Mosko, M., Narayanan, R., Etter, P., Estes, P.S., and Ramaswami, M. 2001. Nucleoside diphosphate kinase, a source of GTP, is required for dynamin-dependent synaptic vesicle recycling. *Neuron* **30**: 197–210.
- Lacombe, M.L., Milon, L., Munier, A., Mehus, J.G., and Lambeth, D.O. 2000. The human Nm23/nucleoside diphosphate kinases. *J. Bioenerg. Biomembr.* **32**: 247–258.
- Lee, T., Hacohen, N., Krasnow, M., and Montell, D.J. 1996. Regulated *Breathless* receptor tyrosine kinase activity required to pattern cell migration and branching in the *Drosophila* tracheal system. *Genes & Dev.* **10**: 2912–2921.
- Lee, J.R., Urban, S., Garvey, C.F., and Freeman, M. 2001. Regulated intracellular ligand transport and proteolysis control EGF signal activation in *Drosophila*. *Cell* **107**: 161–171.
- Leone, A., Flatow, U., VanHoutte, K., and Steeg, P.S. 1993. Transfection of human nm23-H1 into the human MDA-MB-435 breast carcinoma cell line: Effects on tumor metastatic potential, colonization and enzymatic activity. *Oncogene* **8**: 2325–2333.
- Llimargas, M. 1999. The Notch pathway helps to pattern the tips of the *Drosophila* tracheal branches by selecting cell fates. *Development* **126**: 2355–2364.
- MacDonald, N.J., Freije, J.M.P., Stracke, M.L., Manrow, R.E., and Steeg, P.S. 1996. Site-directed mutagenesis of nm23-H1. Mutation of proline 96 or serine 120 abrogates its motility inhibitory activity upon transfection into human breast carcinoma cells. *J. Biol. Chem.* **271**: 25107–25116.
- Manning, G. and Krasnow, M.A. 1993. Development of the *Drosophila* tracheal system. In *The development of Drosophila melanogaster* (ed. M. Bate and A. Martinez Arias), pp. 609–686. Cold Spring Harbor Laboratory Press, Cold Spring Harbor, NY.
- Manoukian, A.S. and Krause, H.M. 1992. Concentration-dependent activities of the even-skipped protein in *Drosophila* embryos. *Genes & Dev.* **6**: 1740–1751.
- Mantrova, E.Y. and Hsu, T. 1998. Down-regulation of transcription factor CF2 by *Drosophila* Ras/MAP kinase signaling in oogenesis: Cytoplasmic retention and degradation. *Genes & Dev.* **12**: 1166–1175.
- Metzger R.J. and Krasnow, M.A. 1999. Genetic control of branching morphogenesis. *Science* **284**: 1635–1639.
- Ohshiro, T. and Saigo, K. 1997. Transcriptional regulation of *breathless* FGF receptor gene by binding of TRACHEALESS/dARNT heterodimers to three central midline elements in *Drosophila* developing trachea. *Development* **124**: 3975–3986.
- Palacios, F., Schweitzer, J.K., Boshans, R.L., and D'Souza-Schorey, C. 2002. ARF6-GTP recruits Nm23-H1 to facilitate dynamin-mediated endocytosis during adherens junctions disassembly. *Nat. Cell Biol.* **4**: 929–936.
- Parks, A.L., Klueg, K.M., Stout, J.R., and Muskavitch, M.A. 2000. Ligand endocytosis drives receptor dissociation and activation in the Notch pathway. *Development* **127**: 1373–1385.
- Perrimon, N., Noll, E., McCall, K., and Brand, A. 1991. Generating lineage-specific markers to study *Drosophila* development. *Dev. Genet.* **12**: 238–252.
- Ribeiro, C., Ebner, A., and Affolter, M. 2002. In vivo imaging reveals different cellular functions for FGF and Dpp signaling in tracheal branching morphogenesis. *Dev. Cell* **2**: 677–683.
- Roymans, D., Willems, R., Van Blockstaele, D.R., and Slegers, H. 2002. Nucleoside diphosphate kinase (NDPK/NM23) and the waltz with multiple partners: Possible consequences in tumor metastasis. *Clin. Exp. Metastasis* **19**: 465–476.
- Sato, M. and Kornberg, T.B. 2002. FGF is an essential mitogen and chemoattractant for the air sacs of the *Drosophila* tracheal system. *Dev. Cell* **3**: 195–207.
- Sawano, A., Takayama, S., Matsuda, M., and Miyawaki, A. 2002. Lateral propagation of EGF signaling after local stimulation is dependent on receptor density. *Dev. Cell* **3**: 245–257.
- Schnepf, B., Donaldson, T., Grumblin, G., Ostrowski, S., Schweitzer, R., Shilo, B.-Z., and Simcox, A. 1998. EGF domain swap converts a *Drosophila* EGF receptor activator into an inhibitor. *Genes & Dev.* **12**: 908–913.
- Sever, S., Muhlberg, A.B., and Schmid, S.L. 1999. Impairment of dynamin's GAP domain stimulates receptor-mediated endocytosis. *Nature* **398**: 481–486.
- Spradling, A.C., Stern, D., Beaton, A., Rhem, E.J., Lavery, T., Mozdén, N., Misra, S., and Rubin, G.M. 1999. The Berkeley *Drosophila* Genome Project gene disruption project: Single P-element insertions mutating 25% of vital *Drosophila* genes. *Genetics* **153**: 135–177.
- Srinivasan, S., Rashka, K.E., and Bier, E. 2002. Creation of a Sog morphogen gradient in the *Drosophila* embryo. *Dev. Cell* **2**: 91–101.
- Steeg, P.S., Bevilacqua, G., Kopper, L., Thorgeirsson, U.P., Talmadge, J.E., Liotta, L.A., and Sobel, M.E. 1988. Evidence for a novel gene associated with low tumor metastatic potential. *J. Natl. Cancer Inst.* **80**: 200–204.
- Steneberg, P., Hemphala, J., and Samakovlis, C. 1999. Dpp and Notch specify the fusion cell fate in the dorsal branches of the *Drosophila* trachea. *Mech. Dev.* **87**: 153–163.
- Sutherland, D., Samakovlis, C., and Krasnow, M.A. 1996. *branchless* encodes a *Drosophila* FGF homolog that controls tracheal cell migration and the pattern of branching. *Cell* **87**: 1091–1101.
- Tanaka-Matakatsu, M., Uemura, T., Oda, H., Takeichi, M., and Hayashi, S. 1996. Cadherin-mediated cell adhesion and cell motility in *Drosophila* trachea regulated by the transcription factor Escargot. *Development* **122**: 3697–3705.
- Teng, D.H., Engele, C.M., and Venkatesh, T.R. 1991. A product of the *prune* locus of *Drosophila* is similar to mammalian GTPase-activating protein. *Nature* **353**: 437–440.
- Timmons, L. and Shearn, A. 2000. Role of AWD/nucleoside diphosphate kinase in *Drosophila* development. *J. Bioenerg. Biomembr.* **32**: 293–300.
- Timmons, L., Hersperger, E., Woodhouse, E., Xu, J., Liu, L.Z., and Shearn, A. 1993. The expression of the *Drosophila awd* gene during normal development and in neoplastic brain tumors caused by *lgl* mutations. *Dev. Biol.* **158**: 364–379.
- Timmons, L., Xu, J., Hersperger, G., Deng, X.F., and Shearn, A. 1995. Point mutations in *awd*^{Kpn} which revert the *prune/Killer of prune* lethal interaction affect conserved residues that are involved in nucleoside diphosphate kinase substrate binding and catalysis. *J. Biol. Chem.* **270**: 23021–23030.
- van der Blik, A.M. and Meyerowitz, E.M. 1991. Dynamin-like protein encoded by the *Drosophila shibire* gene associated with vesicular traffic. *Nature* **351**: 411–414.
- Verveer, P.J., Wouters, F.S., Reynolds, A.R., and Bastiaens, P.I. 2000. Quantitative imaging of lateral ErbB1 receptor signal propagation in the plasma membrane. *Science* **290**: 1567–1570.

Dammai et al.

- Vieira, A.V., Lamaze, C., and Schmid, S.L. 1996. Control of EGF receptor signaling by clathrin-mediated endocytosis. *Science* **274**: 2086–2089.
- Wappner, P., Gabay, L., and Shilo, B.Z. 1997. Interactions between the EGF receptor and DPP pathways establish distinct cell fates in the tracheal placodes. *Development* **124**: 4707–4716.
- Wilk, R., Weizman, I., and Shilo, B.Z. 1996. *trachealess* encodes a bHLH-PAS protein that is an inducer of tracheal cell fates in *Drosophila*. *Genes & Dev.* **10**: 93–102.
- Wolf, C., Gerlach, N., and Schuh, R. 2002. *Drosophila* tracheal system formation involves FGF-dependent cell extensions contacting bridge-cells. *EMBO Rep.* **3**: 563–568.
- Xu, J., Liu, L.Z., Deng, X.F., Timmons, L., Hersperger, E., Steeg, P.S., Veron, M., and Shearn, A. 1996. The enzymatic activity of *Drosophila* AWD/NDP kinase is necessary but not sufficient for its biological function. *Dev. Biol.* **177**: 544–557.
- Yao, Z., Dolginov, Y., Hanoach, T., Yung, Y., Ridner, G., Lando, Z., Zharhary, D., and Seger, R. 2000. Detection of partially phosphorylated forms of ERK by monoclonal antibodies reveals spatial regulation of ERK activity by phosphatases. *FEBS Lett.* **468**: 37–42.



***Drosophila awd*, the homolog of human *nm23*, regulates FGF receptor levels and functions synergistically with *shi/dynammin* during tracheal development**

Vincent Dammai, Boris Adryan, Kim R. Lavenburg, et al.

Genes Dev. 2003 17: 2812-2824

Access the most recent version at doi:[10.1101/gad.1096903](https://doi.org/10.1101/gad.1096903)

Supplemental Material <http://genesdev.cshlp.org/content/suppl/2003/11/07/17.22.2812.DC1.html>

References This article cites 56 articles, 25 of which can be accessed free at:
<http://genesdev.cshlp.org/content/17/22/2812.full.html#ref-list-1>

Email Alerting Service Receive free email alerts when new articles cite this article - sign up in the box at the top right corner of the article or [click here](#).

To subscribe to *Genes & Development* go to:
<http://genesdev.cshlp.org/subscriptions>
